# Multichannel quench-flow microreactor chip for parallel reaction monitoring

**Wojciech P. Bula,*[a] Willem Verboom,[b] David N. Reinhoudt[b] and Han J. G. E. Gardeniers[a]**

*Received 12th July 2007, Accepted 27th September 2007*
*First published as an Advance Article on the web 16th October 2007*
**DOI: 10.1039/b710680g**

This paper describes a multichannel silicon-glass microreactor which has been utilized to investigate the kinetics of a Knoevenagel condensation reaction under different reaction conditions. The reaction is performed on the chip in four parallel channels under identical conditions but with different residence times. A special topology of the reaction coils overcomes the common problem arising from the difference in pressure drop of parallel channels having different length. The parallelization of reaction coils combined with chemical quenching at specific locations results in a considerable reduction in experimental effort and cost. The system was tested and showed good reproducibility in flow properties and reaction kinetic data generation.



## 1. Introduction

Microfluidic systems offer a number of advantages for the field of synthetic chemistry, like enhanced heat and mass transfer.[1,2] The fact that reactions can be performed in complex microchannel networks with volumes of nanolitres or less allows for high-throughput evaluation of (combinatorial) reaction conditions with minute amounts of ingredients of limited availability.[3,4] There is also a significant number of studies reporting the integration of microreactors with analytical instrumentation, allowing monitoring of reaction kinetics on-line or in-line, by NMR,[5] MS,[6] IR,[7] Raman[8] or UV-Vis.[9] The development of a microfluidic parallel reaction network with integrated analysis tools for the on-line determination of reaction kinetics is the goal of our work.

In this paper we describe and analyze the concept of performing a chemical reaction in a microfluidic network that allows the investigation of a reaction at four different reaction times simultaneously. This multichannel reactor offers a promising alternative to single-channel T-type devices because of a serious reduction in experimentation effort and expenses (*e.g.*, using a minimal number of pumps), and furthermore provides more precise data due to the fact that the reaction in every channel is performed under identical conditions. The concept can be easily extended to a higher number of reaction channels in parallel, in which case a wide range of residence time points on a reaction kinetic curve can be covered just by a single flow rate.

## 2. Chip design

The microreactor is unique in that it combines the parallelization of chemical reactions with integrated reactant mixing and reaction quenching functionalities. Fig. 1 gives a schematic overview of the investigated quench-flow microreactor with parallel reaction lines.

A chemical reaction is initiated in a mixer, and the reacting mixture is subsequently equally distributed over four reaction coils with a different residence time (here arranged by different

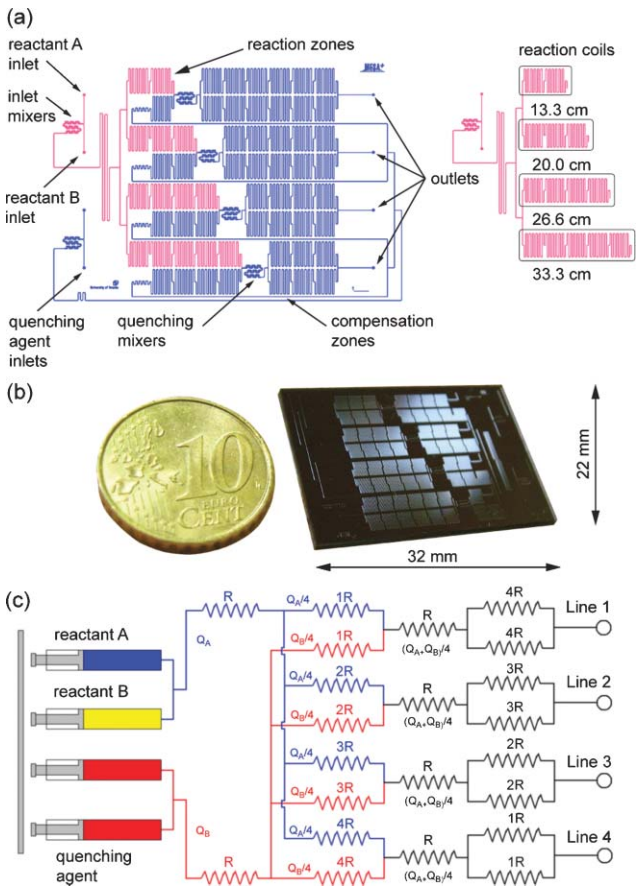


**Fig. 1** (a) Schematic representation and functional structure of the multichannel quench-flow microreactor. (b) Photo of the microfluidic chip in comparison with a 10 Eurocent coin. (c) The hydraulic model of the 4 lines chip.

[a]*Mesoscale Chemical Systems, MESA+ Institute for Nanotechnology, University of Twente, P.O. Box 217, 7500 AE, Enschede, The Netherlands. E-mail: w.p.bula@utwente.nl; Fax: +31 534891096; Tel: +31 534892594*
[b]*Supramolecular Chemistry and Technology (SMCT) Group, MESA+ Institute for Nanotechnology, University of Twente, P.O. Box 217, 7500 AE, Enschede, The Netherlands*

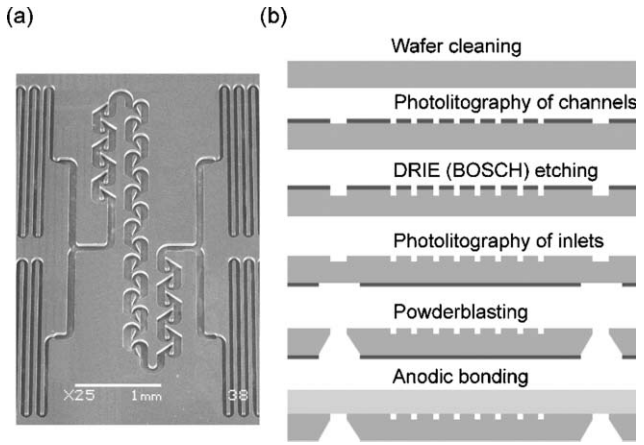


**Fig. 2** (a) SEM image of quenching mixer. (b) Process scheme for the fabrication of the microreactor (not to scale). See text for details.

coil lengths). At the end of each coil, the reaction is quenched chemically in a micromixer. Subsequently, the quenched mixtures pass through different coils, of which the main purpose is to compensate for differences in flow resistance between the lines, so that the system can be controlled by only three pumps (reactants A and B and quenching agent). The reaction time for each line is defined as the period between the process initialization in the inlet mixer and the reaction termination in the quenching mixers and is varied through the experiment by changing the inlet pumping rates. Mixing times are typically 2% of the residence time in the reaction coils. Customized in-plane passive micromixers with modified Tesla structures, as proposed by Hong *et al.*,[10] were implemented on the chip (Fig. 2a).

The outlet of each line was designed to match the format of a sample plate for MALDI-MS. The MALDI matrix compound could be mixed in with the quenching substance (in some cases the MALDI matrix itself can act as a quenching agent). In this study, we focus only on the parallelization concept, MALDI work is in progress. For proof of principle of the parallel coil concept, the conversion in each line was monitored by external UV-Vis absorbance after collection of fractions at the outlet of each reaction coil.

## 3. Experimental

### 3.1 Microfabrication procedure

The silicon-glass microreactor was fabricated by standard microfabrication processes.[11] The process for the fabrication of the chip is presented schematically in Fig. 2b.

The channels were formed in 4 inch (100) silicon wafers by deep reactive ion etching (BOSCH-type process) using a mask of photoresist. Inlet holes were fabricated using powder-blasting. The silicon wafer was anodically bonded to Pyrex glass ($T$ = 400 °C, $U_{max}$ = 1000 V, $t$ = 20 min) and the silicon-glass stack was diced into separate chips. The use of only (oxidized) silicon and glass makes the chip compatible with a wide range of organic solvents and reaction temperatures. Channel dimensions are 50 μm × 53 μm (width × depth). The shortest reaction coil is built of 2 segments, the longest one of 5 segments. The length of a single segment is 6.64 cm. The total

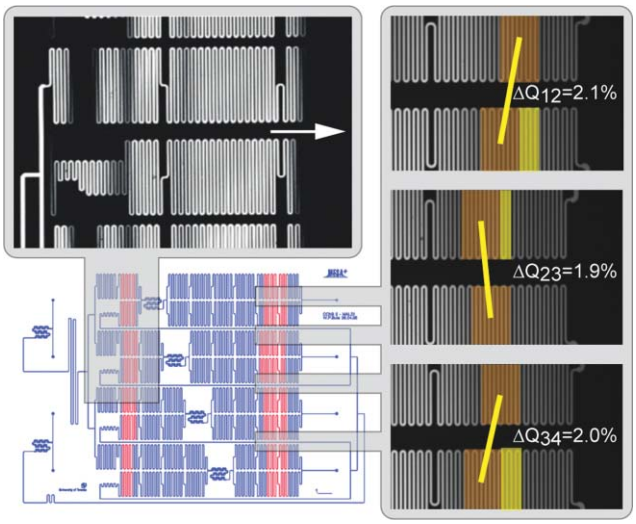


**Fig. 3** Transport of fluorescent plugs in parallel reaction loops and in the quenching zone.

microreactor volume is 16 μL, of which 2.2 μL is the original reaction mixture in 4 coils (0.35, 0.53, 0.70 and 0.88 μL).

### 3.2 Flow parallelization tests

Flow parallelization tests were performed by observing the transport of fluorescent dye plugs through parallel channels for various flow rates. A 0.1 mM solution of fluorescein sodium salt in acetonitrile was used as a marker. Differences between the flows in complementary channels were measured to be smaller than 4% for the tested flow rate range (0.1 to 2 μL $min^{-1}$) (Fig. 3).

Differences were found to be caused by non-uniformity of silicon etching, resulting in different channel depths across the chip. In this respect it has to be mentioned that channel depth or width differences are amplified in the flow rate due to the fact that the hydraulic resistance is proportional to the square of both the depth and the width. For example, a depth variation of 1 μm on a nominal channel depth of 50 μm will give rise to the measured 4% flow variation. Such a variation of 2% in etching rate over a 4 inch wafer is not uncommon and depends on feature size and locally exposed etched surface area (loading).[12]

### 3.3 Kinetic model of the reaction

As a test reaction the Knoevenagel condensation reaction of 4-methoxybenzaldehyde (**1**) with propanedinitrile (**2**) in the presence of 1,8-diazabicyclo-[5.4.0]undec-7-ene (DBU) as a base was studied (Scheme 1). This reaction has been studied several times before in various types of microreactors.[13–15]

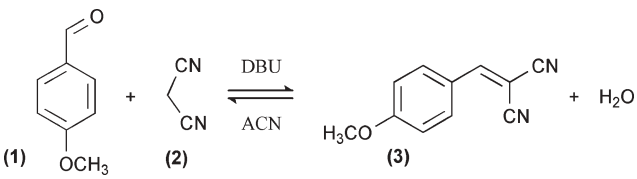


**Scheme 1** Scheme of the condensation reaction of 4-methoxybenzaldehyde and propanedinitrile.

 

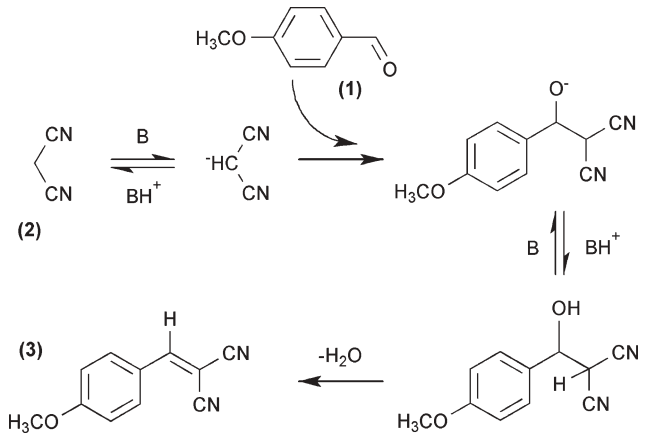

**Scheme 2** Classical reaction scheme for base catalyzed Knoevenagel condensation reaction.

Considering the addition of the enolate anion onto 4-methoxybenzaldehyde as the rate-limiting step in the reaction (Scheme 2), the following second-order reversible reaction scheme can be applied.[16] With the restrictions that initial concentrations of reactants are equal and there are no products initially present, the rate equation is given by:[17]

$$\frac{dC_A}{dt} = \frac{dC_P}{dt} = C_{A0}\frac{dX_A}{dt} = k_1 C_A^2 - k_2 C_P^2 = \\ = k_1 C_{A0}^2 (1 - X_A)^2 - k_2 X_A^2 C_{A0}^2 \quad (1)$$

where $C_A$ is concentration of reactant, $C_{A0}$ – initial concentration of reactant, $C_P$ – concentration of product, $X_A$ – fractional conversion $X_A = (C_{A0} - C_A)C_{A0}^{-1}$, $X_{Ae}$ – fractional conversion at equilibrium $X_{Ae} = (C_{A0} - C_{Ae})C_{A0}^{-1}$, $C_P$ – concentration of product $C_P = X_A C_{A0}$, and the fractional conversion $X_A = 0$ at $t = 0$.

At equilibrium, $dX_A/dt = 0$ and the solution of differential eqn (1) is:

$$\ln\left(\frac{X_{Ae} - (2X_{Ae} - 1)X_A}{X_{Ae} - X_A}\right) = 2k_1 C_{A0}\left(\frac{1}{X_{Ae}} - 1\right)t \quad (2)$$

By expressing $X_A$ and $X_{Ae}$ by $C_A$ and $C_{Ae}$, the integrated rate equation, rearranged with respect to the concentration of product, $C_P$ is given by:

$$C_P = \frac{C_{A0}(A-1)(C_{A0} - C_{Ae})}{C_{A0}(A-1) + 2C_{Ae}} \\ A = \exp\left(\frac{2k_1 C_{A0} C_{Ae}}{C_{A0} - C_{Ae}}t\right) \quad (3)$$

where $C_{A0}$ is the initial concentration of the reactant and $C_{Ae}$ is the concentration of the reactant at equilibrium.

### 3.4 Experimental procedure

Prior to an experiment, the chip was placed in an in-house fabricated holder and connected to syringes by fused silica capillary tubes. Subsequently, the microreactor was flushed with acetonitrile (ACN) to remove air trapped inside the channels. Next, the syringes with reactants were connected to the microreactor and the device was filled with reagents. The desired flow rate and reaction conditions were set, the chip was flushed again, and the sample collection started.

The temperature of the microreactor was controlled by interfacing a thermoelectric module with a heat sink and copper plate with the chip. Temperature variation on the glass surface of the chip measured with a thermocouple was less than 0.1 K.

The reactants were equimolar (40 mM) solutions of **1** and **2** in ACN. The reaction starts in the inlet mixer when the reactant mixture from syringe 1 combines in equal ratio with the base DBU, acting as a catalyst, from syringe 2. The reaction was performed for DBU concentrations of 4, 8, 12 and 16 mM. Quenching consists of mixing the reaction mixture 1 : 1 with 2,2,2-trifluoroacetic acid (TFA). The molar ratio between TFA and DBU was higher than 12.5 during the experiments in order to perform quenching in negligible time. This ratio resulted from a series of microreactor experiments in which off-line UV measurements were performed on reaction mixtures, to which TFA of different concentrations was added. Additional control experiments showed that there is no conversion if DBU is not present in the chemical system. It was also found experimentally that without DBU but with TFA, no conversion takes place.

The minimal volume of the sample collected for analysis was 8 μL. The eluents were collected in sealed glass vials cooled down to −10 °C to prevent solvent evaporation. The theoretical maximum molar concentration of product in the output eluent is 10 mM, due to the double dilution that takes place on the chip.

Conversion of the reactants to 2-[(4-methoxyphenyl)methylidene]propanedinitrile (**3**) (PMB) in the four reaction coils was monitored by off-line absorbance measurements, based on the decrease of the characteristic UV peak for **1** and the increase of the product peak. The absorbance measurements of the reaction products were performed at a wavelength of 345 nm on a Varian Cary 300 spectrophotometer. Four kinetic points related to four reaction times (up to 4 min) were collected for pump flow rates of 0.5, 1.0 and 2.0 μL $min^{-1}$ per inlet.

## 4. Results and discussion

### 4.1 Kinetic studies of Knoevenagel condensation

The reaction was carried out in the microreactor at temperatures between 40 and 60 °C. The experiments were performed with 40 mM solutions of the reactants and different catalyst concentrations in the range from 4 mM to 16 mM.

The Levenberg–Marquardt error minimization algorithm[18,19] was utilized to minimize the conversion function (eqn (3)) in order to fit the kinetic curves into data representing the formation of reaction products (Fig. 4 and Fig. 5).

The rate constants and reactant concentrations at equilibrium for different reaction conditions (Table 1) were calculated from the model. The $R^2$ representing the fitting quality stays within the range 0.97–0.99. A directly proportional relationship between the value of the reaction constant and catalyst concentration was observed.

To calculate the activation energy of the reaction catalyzed by a 12 mM solution of DBU, the experiments performed at 50 °C were repeated at different temperatures. An activation

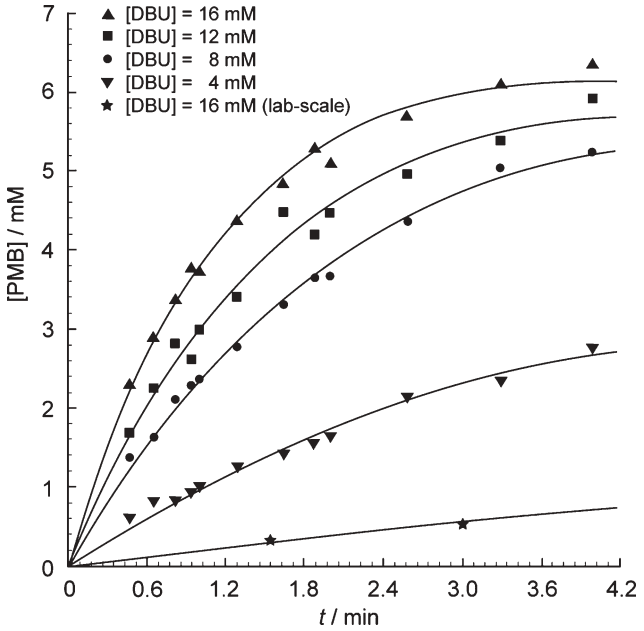


**Fig. 4** Kinetic curves of the on-chip and lab-scale experiments fitted to measurement points for different concentrations of catalyst ($T$ = 50 °C). Samples of the -scale experiment were collected over 30 min with 3 min intervals (not shown on the plot).

energy $E_a$ = 60 kJ·mol$^{-1}$ and a reaction frequency factor $A = 6 \times 10^{10}$ M$^{-1}$ min$^{-1}$ were calculated from the fitted Arrhenius equation. The standard deviation in product concentration (based on 3 independent experiments) was <2.5%, thereby showing the reproducibility of the method.

For comparison, the reaction was performed in a conventional laboratory-scale batch reactor set-up, with identical residence time, temperature, concentrations, and detection method. The reaction of premixed **1** and **2** was initiated in glassware by addition of the catalyst at 50 °C. Samples were collected over 30 min with 3 min intervals from a constantly stirred mixture and immediately quenched by mixing with an identical volume of quenching solution, with a TFA to DBU ratio of 50. Eight microlitres of the quenched sample was analyzed by UV-Vis spectrophotometry. By following the reaction for 5, 10 and 15 min after quenching, it was found that the used quenching method was indeed efficient. For analysis, the same kinetic model as for the chip experiments was used.

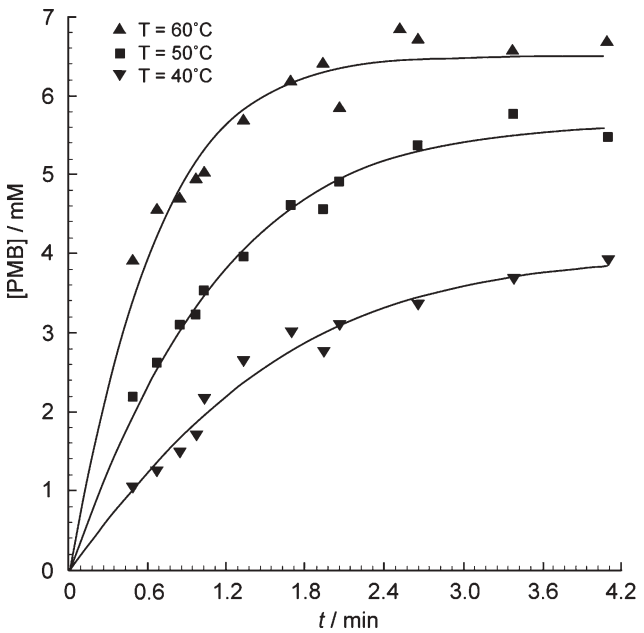


**Fig. 5** Kinetic curves of the on-chip experiments fitted to measurement points for different temperatures ([DBU] = 12 mM).

**Table 1** Reaction conditions and fitted reaction parameters

| $C_{Cat}$[a]/mM | Method | $T$/°C | $k_f$[b]/M$^{-1}$ min$^{-1}$ | $k_r$[c]/M$^{-1}$ min$^{-1}$ | $C_{Pe}$[d]/mM |
|---|---|---|---|---|---|
| 4 | Chip | 50 | 2.3 | 1.0 | 6.0 |
| 8 | Chip | 50 | 6.6 | 2.9 | 6.1 |
| 12 | Chip | 50 | 9.1 | 4.0 | 6.1 |
| 16 | Chip | 50 | 13.1 | 5.8 | 6.1 |
| 12 | Chip | 40 | 5.7 | 1.4 | 3.9 |
| 12 | Chip | 50 | 10.6 | 4.4 | 5.9 |
| 12 | Chip | 60 | 23.0 | 10.8 | 6.4 |
| 16 | Batch | 50 | 0.49 | 0.21 | 1.9 |

[a] $C_{Cat}$ – concentration of catalyst, [b] $k_f$ – forward reaction constant, [c] $k_r$ – reverse reaction constant, [d] $C_{Pe}$ – concentration of product at equilibrium.

A remarkable result is that the conversion values and the reaction rates found for the chip experiments are substantially higher than those obtained in the lab-scale batch experiments (Table 1).

This conclusion also stands if the fundamental differences between the two reactor types (plug flow for the chip and stirred tank for the lab-scale reactor) are taken into account. A higher conversion on-chip, compared to lab-scale, has consistently been found in our lab, also for reactions in which no catalyst was involved;[5] the latter rules out the potential influence of surface catalytic effects.[20] In order to use the chip reaction kinetic system in an industrial research environment, for example, to quickly screen reaction concentration and temperature conditions, it is important that chip reaction kinetic data can be translated reliably to larger scale reaction systems, for which industrial scale-up rules have been established.

### 4.2 Estimation of the residence time distribution

The residence time distribution, RTD, for species in a microchannel flow reactor is the result of the combination of convection and diffusion of species. In our work, the RTD serves as an estimate of the accuracy of reaction kinetic data, as presented above. More generally, the RTD is of importance for the selectivity of reactions, in cases where byproducts are expected. Below, we will make an estimation of the RTD in our experiments.

The transport of a plug of tracers by a pressure-driven flow through a tube was first studied by Taylor and Aris.[21] They derived that for long residence times, where the concentration has become homogeneous in the cross-sectional plane, the axial tracer distribution evolves diffusively with a long-time dispersivity, $D_{eff}$, described by the equation:[22]

$$D_{eff} = D\left(1 + \frac{1}{210} Pe^2 f\left(\frac{d}{W}\right)\right) = D\left(1 + \frac{1}{210}\left(\frac{UW}{D}\right)^2 f\left(\frac{d}{W}\right)\right) \quad (4)$$

 

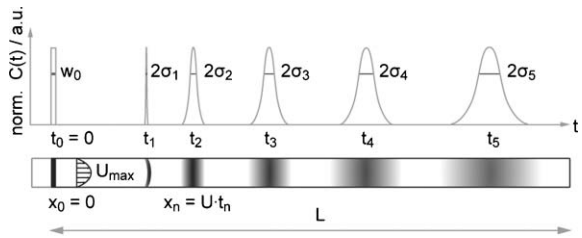


**Fig. 6** A schematic representation of a plug undergoing dispersion in a straight microchannel. The shape of the concentration distribution approaches the Gaussian distribution for $t \rightarrow \infty$.

where $f(d/W)$ is a function which depends on the geometry of the channel cross-section, $Pe$ is the Péclet number, $W$ and $d$ are channel width and depth, respectively. The function $f(d/W)$ approaches a value of about 1.76 as $d/W \rightarrow 1$ for a square channel in case of Taylor dispersion with a parabolic velocity profile.

A definition of "long residence time" follows from the following: under a pressure-driven flow an ideal input pulse (δ-Dirac function) in a channel of width $W$ is convectively stretched into a parabolic shape, where width increases linearly with time. After a characteristic time scale $\tau_D \sim w^2/D$ for tracer to diffuse across the channel, the parabolic profile is diffusively smoothed into a plug of a Gaussian longitudinal concentration distribution. Fig. 6 gives an illustration of this. It shows the evolution of a tracer concentration profile along the center of the microfluidic channel, expressed in terms of the standard deviation $\sigma$ of residence time (see below).

The characteristic time $\tau_D$ corresponds to a length $W_{TD} \sim Uw^2/D$ and implies that eqn (4) is valid if the coil is longer than $W_{TD}$. For channels of width 50 μm, this length is about 3.9 mm and 16.7 mm for $U$ = 1.57 mm $s^{-1}$ and $U$ = 6.67 mm $s^{-1}$, respectively ($D = 1 \times 10^{-9}$ $m^2$ $s^{-1}$). From this it follows that the "long residence time" condition is valid in our experiments.

In our case the degree of dispersion is measured in terms of the standard deviation of the species concentration profile. In case the Dirac-pulse is used as an initial condition:

$$C(t=0) = \frac{N_0}{\pi a^2}\delta(t) \tag{5}$$

the concentration profile is defined by the following equation:[23]

$$C(t) = \frac{N_0}{\pi a^2}\frac{1}{\sqrt{4\pi D_{\text{eff}} t_{\text{nom}}}}\exp\left(-\frac{U^2(t_{\text{nom}}-t)^2}{4D_{\text{eff}} t_{\text{nom}}}\right) \tag{6}$$

where $t_{nom}$ is the nominal residence time defined as the residence time of the maximum in the concentration profile, $a$ is the radial characteristic length, $N_0$ represents the number of tracer moles in excess of those present in the same volume of the flowing stream, and $U$ stands for a mean velocity. The $2\sigma$ width corresponds to 0.607 of concentration peak maximum of the Gaussian distribution ($t = t_{nom}$).

The dispersion in a meandering channel differs from the dispersion in a straight one. Solute moving at the maximum velocity in a curved channel (near inner wall) has a shorter distance to move to reach any axial position than solute moving near the outer wall. Curvature increases the variation in residence time across the flow and this results in the increase of the dispersion coefficient $D_{eff}$ in case of curved channels.

The influence of curvature in meandering channels on the dispersion effects can be evaluated by calculating the $Dn^2Sc$ criterion based on dimensionless Dean ($Dn$) and Schmidt ($Sc$) numbers. According to the work of Johnson and Kamm,[24] secondary flow effects start to affect the dispersion process for $Dn^2Sc > 100$. The criterion quantity for our experiments are approximately 20, 95 and 375 for linear velocities of 1.57, 3.33 and 6.67 mm $s^{-1}$, respectively, which suggests that the influence of the curves in the channel can not be neglected.

According to work of Nunge *et al.*,[25] the normalized dispersion coefficient is proportional to the Péclet number and inversely proportional to curvature ratio $\lambda = r/W$, where $r$ is the radius of curvature. From their work it can be derived that the ratio between the dispersion coefficient in a curved channel ($D_{effC}$) to the one in a straight system ($D_{eff}$) is about 5 for $\lambda = 1.8$ and $Pe > 70$.

The total system variance $\sigma^2$ of the residence time is the sum of the contributions from the straight and curved parts of the reaction coil independently. $D_{effC}$ has been used to calculate the standard deviation of residence time in a single turn and from that we calculate the total variance of all curvatures in the reaction coil. A similar procedure was conducted for the estimation of variance in straight parts of the reaction coil. The square root of total variance is the standard deviation of RTD.

It was calculated that in the microreactor channel for an average residence time of 4 min, the standard deviation of the residence time distribution, based on Taylor dispersion alone, is *ca.* 7 s, an error of only 3% on the total residence time (Fig. 7). Assuming that 99.99% of molecules have a residence time within the range of $4\sigma$, the corresponding total plug width is about 28 s (for an estimated molecular diffusion coefficient $D = 1 \times 10^{-9}$ $m^2$ $s^{-1}$). This, in combination with the medium–high Péclet numbers of *ca.* 70 to 340 calculated for our experiments, gives confidence that the calculation of residence times based on ideal plug flow behaviour, as was done in our evaluation of the data, is basically correct. More detailed

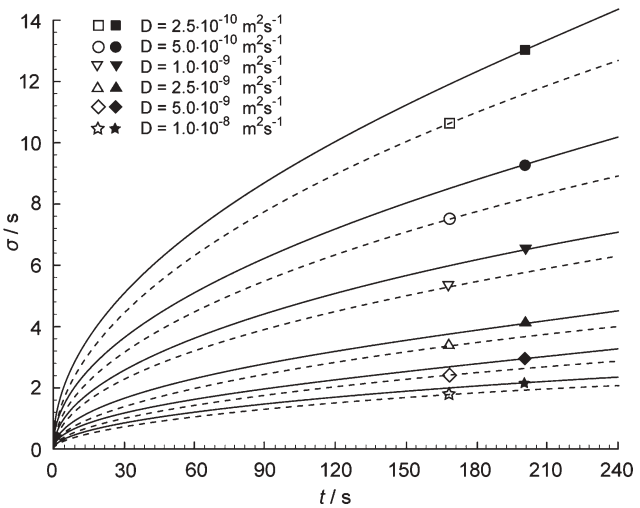


**Fig. 7** Plot of standard deviation of RTD in a straight channel (dashed line) and in a meandering channel (solid line), as a function of residence time for different values of the mass diffusion coefficient.

experimental work, combined with a full mathematical treatment of the reaction–diffusion problem in a continuous-flow microchannel reactor as used here, is currently in progress.

## 5. Conclusions

In conclusion, we have clearly demonstrated that silicon-glass microreactors containing parallel lines allow the accurate investigation of the kinetics of a reaction at different reaction times. In addition to reactant volumes less than 1 μL, there is a considerable reduction in experimental effort.

The topology of the presented microreactor allows the diversification of reaction times, by introduction of an inhibitor into reaction lines at different locations, without disturbing the flow regime. A chip with 4 parallel reaction lines was tested in detail, but microreactors with 8, 16 and more parallel lines can be easily designed, fabricated and applied for kinetic studies using the same concept. Flow parallelization tests showed that the differences in flow rates between lines are small enough to obtain precise reaction kinetic data.

For the reactions in the chip, significantly higher rate constants were found, compared to lab-scale experiments. We attribute the nature of this phenomenon to the mass transport limitations in the lab-scale experiments, these limitations are absent in the microreactors. The implementation of various functionalities as fluid control, reaction line parallelization and quenching within one microchip reduces the number of parameters that could decrease the precision of the microscale effects investigation.



## Acknowledgements

We acknowledge financial support from the Netherlands Organisation for Scientific Research and Advanced Chemical Technologies for Sustainability (NWO-ACTS) through the Process-on-a-Chip program.

## References

1 K. F. Jensen, *Chem. Eng. Sci.*, 2001, **56**, 293.
2 K. Jähnisch, V. Hessel, H. Löwe and M. Baerns, *Angew. Chem.*, 2004, **116**, 410, (*Angew. Chem., Int. Ed.*, 2004, **43**, 406).
3 H. Song, D. L. Chen and R. F. Ismagilov, *Angew. Chem.*, 2006, **118**, 7494, (*Angew. Chem., Int. Ed.*, 2006, **45**, 7336).
4 C. L. Hansen, S. Classen, J. M. Berger and S. R. Quake, *J. Am. Chem. Soc.*, 2006, **128**, 3142.
5 H. Wensink, F. Benito-Lopez, D. C. Hermes, W. Verboom, J. G. E. Gardeniers, D. N. Reinhoudt and A. van den Berg, *Lab Chip*, 2005, **5**, 280.
6 M. Brivio, R. H. Fokkens, W. Verboom, D. N. Reinhoudt, N. R. Tas, M. H. Goedbloed and A. van den Berg, *Anal. Chem.*, 2002, **74**, 3972; M. Brivio, N. Tas, M. H. Goedbloed, H. J. G. E. Gardeniers, W. Verboom, A. van den Berg and D. N. Reinhoudt, *Lab Chip*, 2005, **5**, 378.
7 R. Herzig-Marx, K. T. Queeney, R. J. Jackman, M. A. Schmidt and K. F. Jensen, *Anal. Chem.*, 2004, **76**, 6476; T. M. Floyd, M. A. Schmidt and K. F. Jensen, *Ind. Eng. Chem. Res.*, 2005, **44**, 2351.
8 P. D. I. Fletcher, S. J. Haswell and X. Zhang, *Electrophoresis*, 2003, **24**, 3239.
9 R. J. Jackman, T. M. Floyd, R. Ghodssi, M. A. Schmidt and K. F. Jensen, *J. Micromech. Microeng.*, 2001, **11**, 263; R. M. Tiggelaar, T. T. Veenstra, R. G. P. Sanders, J. G. E. Gardeniers, M. C. Elwenspoek and A. van den Berg, *Talanta*, 2002, **56**, 331; J.-S. Park, K.-B. Park, K.-S. Shin, H.-D. Park, M.-C. Kim, J.-R. Kim, S.-J. Park and Y.-H. Song, *Sens. Actuators, B*, 2006, **117**, 516.
10 C.-C. Hong, J.-W. Choi and C. H. Ahn, *Lab Chip*, 2004, **4**, 109.
11 J. G. E. Gardeniers, R. E. Oosterbroek and A. van den Berg, Silicon and glass micromachining for μTAS, in: *Lab-on-a-chip: Miniaturized systems for (bio)chemical analysis and synthesis*, ed. R. E. Oosterbroek and A. van den Berg, Elsevier, Amsterdam, 2003, pp. 37–64.
12 A. A. Ayón, R. Braff, C. C. Lin, H. H. Sawin and M. A. Schmidt, *J. Electrochem. Soc.*, 1999, **146**, 339.
13 A. R. Bogdan, B. P. Mason, K. T. Sylvester and D. T. McQuade, *Angew. Chem., Int. Ed.*, 2007, **46**, 1698.
14 C. Wiles, P. Watts and S. Haswell, *Chem. Commun.*, 2007, 966.
15 C. Wiles, P. Watts and S. Haswell, *Lab Chip*, 2007, **7**, 322.
16 X. Zhang, E. S. M. Lai, R. Martin-Aranda and K. L. Yeung, *Appl. Catal., A*, 2004, **261**, 109.
17 A. K. Coker, *Modeling of chemical kinetics and reactor design*, Butterworth-Heinemann, Woburn, 2001, pp. 150.
18 K. Levenberg, *Quart. Appl. Math.*, 1944, **2**, 164.
19 D. Marquardt, *J. Soc. Ind. Appl. Math.*, 1963, **11**, 431.
20 M. Brivio, R. E. Oosterbroek, W. Verboom, M. H. Goedbloed, A. van den Berg and D. N. Reinhoudt, *Chem. Commun.*, 2003, 1924.
21 G. Taylor, *Proc. R. Soc. London, Ser. A*, 1953, **219**, 186; R. Aris, *Proc. R. Soc. London, Ser. A*, 1956, **235**, 67.
22 D. Dutta, A. Ramachandran and D. T. Leighton, Jr, *Microfluid. Nanofluid.*, 2006, **2**, 275.
23 J. Crank, *The Mathematics of the diffusion*, Oxford University Press, 1975; A. Alizadeh, C. A. Nieto de Castro and W. A. Wakeham, *Int. J. Thermophys.*, 1980, **1**(3), 243.
24 M. Johnson and R. D. Kamm, *J. Fluid Mech.*, 1986, **172**, 329.
25 R. J. Nunge, T.-S. Lin and W. N. Gill, *J. Fluid Mech.*, 1972, **51**, 363.

 